Supporting Information

Boghaert et al. 10.1073/pnas.1118872109

SI Methods

Cell Culture and Reagents. Functionally normal EpH4 mouse mammary epithelial cells and SCg6 mouse mammary tumor cells were cultured in 1:1 Dulbecco's modified Eagle's medium: Ham's F 12 nutrient mixture (DMEM:F12; HyClone), 2% (vol/vol) FBS (Atlanta Biologicals), 5 μg/mL insulin (Sigma), and 50 μg/mL gentamicin (Sigma). D920 human mammary progenitor cells (1, 2) were cultured on collagen-coated tissue culture dishes in DMEM:F12, 250 ng/mL insulin, 10 μg/mL transferrin (Sigma), 2.6 ng/mL sodium selenite (Sigma), 0.1 nM estradiol (Sigma), 1.4 μM hydrocortisone (Sigma), 5 μg/mL prolactin (Sigma), and 50 μg/mL gentamicin. MDA-MB-231 human breast tumor cells were cultured in DMEM:F12, 10% (vol/vol) FBS, and 50 μg/mL gentamicin. All other breast tumor cell lines (4T1, Hs578T, etc.) were cultured in DMEM (Gibco), 10% (vol/vol) FBS, and 50 μg/mL gentamicin.

To generate 3D tissues, elastomeric stamps of poly(dimethylsiloxane) (Sylgard 184, Ellsworth Adhesives) were coated with 1% (wt/vol) BSA in PBS. A drop of neutralized native type I collagen (Koken) was placed on each stamp. The stamps were inverted, and the collagen was gelled at 37 °C. The stamps were then gently removed, and a suspension of cells was allowed to settle within the wells. Extra cells were washed away with culture medium, and flat collagen gelled against a coverslip was placed on top of the sample. The initial position of the tumor cell was recorded after tissue construction. Samples were fixed 48 h later using 4% (wt/vol) paraformaldehyde in PBS and imaged to determine the final position of the tumor cell.

Tissues were treated with the following reagents diluted to the concentrations indicated: GM6001 (40 μM; Calbiochem); AG1478 (80 nM; Tocris); calyculin A (0.1 nM; Calbiochem); Y27632 (10 μM; Tocris); and blebbistatin (25 μM; Sigma).

Tissues were stained for adherens junctions using rabbit anti-β-catenin (Sigma) or rabbit anti-E-cadherin (Cell Signaling), filamentous actin using Alexa 488-conjugated phalloidin (Invitrogen), apical polarity using rabbit anti-ZO-1 (Zymed), activated focal adhesion kinase (FAK) using rabbit anti-FAK [pY^{397}] (Invitrogen), and β1-integrin using mouse anti-integrin β1 (Abcam).

Recombinant adenoviruses encoding $RhoA^{N19}$ and $RhoA^{L63}$ were obtained from Cell Biolabs. Recombinant adenoviruses encoding human E-cadherin lacking the β-catenin-binding domain (EΔ) and mutant FAK lacking the autophosphorylation site (FAK-Dter) were prepared as described previously (3). Mammary epithelial cells were transduced at 100 viral particles per cell for 24 h. Cells were then washed and incorporated into tissues.

The autoclustering β1-integrin mutant ($\beta1^{V737N}$) was generated using the QuikChange Lightening site-directed mutagenesis kit (Stratagene). Cells were transfected using Fugene HD according to the manufacturer's protocol (Roche).

Transgenic Mouse Model and Preparation of Mammary Gland Whole Mounts. Mice were housed in pathogen-free conditions according to protocols approved by the Institutional Animal Care and Use Committee at the Mayo Clinic. To induce *TetO-kRas* transgene expression, the mice were fed doxycycline (Bio-Serv) at a concentration of 200 mg/kg. After 2 d of treatment, mice were killed by CO_2 asphyxiation. The inguinal mammary glands were removed and prepared for whole mount by fixation in Carnoy's solution followed by staining with carmine aluminum.

Labeling Tumor Cells. Recombinant adenoviruses encoding H2B-mCherry (Vector Biolabs) and LifeAct-GFP (Vector Biolabs) were used to label the nuclei and actin of the tumor cells, respectively. Cells were transduced sequentially with H2B-mCherry adenovirus and LifeAct-GFP adenovirus at 100–150 viral particles per cell. Labeled tumor cells were incorporated into tissues 12–16 h after viral transduction.

Analysis of Invasion. Percent invasion ($\%I$) was calculated by determining the number of tumor cells at a given initial location that had invaded (I) and the number of tumor cells that did not invade (N) $\%I = \frac{I}{I+N} \times 100$.

Tumor Cell Proliferation and Turnover. The fraction of proliferating cells was assessed by examining incorporation of the thymidine analog 5-ethynl-2′-deoxyuridine (EdU) using the Click-iT EdU Alexa Fluor 488 Imaging Kit (Invitrogen) according to the manufacturer's protocol. Tumor cell turnover was determined by counting the final number of tumor cells in tissues in which there was initially a single tumor cell. Tissues with a final tumor cell count of 0 were labeled as "Net Cell Death," tissues with a final tumor cell count of 1 were labeled as "No Change," and tissues with a final tumor cell count of 2 or more were labeled as "Net Proliferation."

Bead Displacement Experiments. Displacement maps of the collagen gel were created by imaging the position of 1-μm diameter fluorescent beads (Invitrogen) before and after relaxing the tissue with 0.1% (wt/vol) Triton-X-100 in PBS as previously described (3). Bead displacement was calculated using Imaris tracking software (Bitplane). Frequency maps were generated using a custom MATLAB code that rasters spatially back and forth through a grid of points and calculates the mean displacement at those points from n displacement maps, thus producing a map depicting the average displacements at each position relative to the center point of the tubule (bump geometry) or center point between the tubules.

Microcomputed Tomographic Analysis. Inguinal mammary glands were harvested from 8-wk-old CD1 mice (Charles River). The glands were fixed in Carnoy's solution (75% ethanol/25% glacial acetic acid), dehydrated, and cleared with toluene. Glands were then rehydrated and soaked in Lugol's iodine solution (Sigma) as a contrast agent for 3 d with daily solution changes (4). The samples were embedded in paraffin wax and scanned in an eXplore Locus SP specimen scanner (GE Healthcare) with 16-μm isotropic spatial resolution. ImageJ (National Institutes of Health) was used to reconstruct microcomputed tomographic (μCT) images. ItkSNAP (open source; itksnap.org) was used to segment the epithelial tree and tissue boundaries and fit isosurfaces according to size-thresholding and region-growing algorithms. Curvature continuous surfaces were generated with Blender v2.5 (open source; blender.org) to smooth and create a continuous closed topology. Because of the complexity of the geometry and the number of vertices needed to represent the surface mesh, two volumes from different regions of the gland (middle and end) were selected for analysis. Computer-assisted design (CAD) solid models were constructed from these sampling volumes using Inventor 2011 (Autodesk), whereby the surface model was used to define the geometry and the cross-sectional area along the lengths of the ducts.

Numerical Modeling. A 3D computational model of the surrogate tissues and mammary ducts was solved to calculate the spatial pattern of endogenous mechanical stress using the finite element method, as described previously (3, 5). The surrogate tissues or ducts of the mammary gland were modeled in Comsol Multi-

physics v4.1 software as hollow contractile shells 10 μm thick (6) with a Young's modulus of 500 Pa (7) and a near-incompressible Poisson ratio of 0.499 (3). As a first-order approximation, the ECM was modeled as a collagen matrix and treated as a continuous linearly elastic solid with a bulk Young's modulus of 300 Pa (8) and Poisson ratio of 0.2 (9). Recent experiments have demonstrated that in the surrogate tissues, the epithelial cells remodel the collagen matrix, preferentially increasing the Young's modulus at the tips of these tissues (5). To estimate these spatial heterogeneities in the collagen modulus, the modulus at the tips of the tissues was defined at the tissue/collagen interface as four times higher than the bulk modulus ($E_{max} = 4 \cdot E_{bulk}$), exponentially decaying (with a decay rate, $k = 6.25e^{4}$) to the bulk modulus at a distance R away from the tissue ($E = E_{bulk} + E_{max}e^{-kR}$). The outer surface of the collagen matrix far from the embedded epithelial tissue was fixed, and the inner surface of the hollow epithelial shell was traction free. An isotropic thermal strain was imposed on the epithelial shell to model isometric contraction of the epithelium arising from cellular contractility (3). The resulting spatial patterns of maximum principal stress within the ECM or at the epithelial surface were calculated.

1. Gudjonsson T, et al. (2002) Isolation, immortalization, and characterization of a human breast epithelial cell line with stem cell properties. *Genes Dev* 16(6):693–706.
2. LaBarge MA, et al. (2009) Human mammary progenitor cell fate decisions are products of interactions with combinatorial microenvironments. *Integr Biol (Camb)* 1(1):70–79.
3. Gjorevski N, Nelson CM (2010) Endogenous patterns of mechanical stress are required for branching morphogenesis. *Integr Biol (Camb)* 2(9):424–434.
4. Degenhardt K, Wright AC, Horng D, Padmanabhan A, Epstein JA (2010) Rapid 3D phenotyping of cardiovascular development in mouse embryos by micro-CT with iodine staining. *Circ Cardiovasc Imaging* 3(3):314–322.
5. Gjorevski N, Nelson CM (2012) Mapping of mechanical strains and stresses around quiescent engineered three-dimensional epithelial tissues. *Biophys J* 103(1):152–162.
6. Khaled WT, et al. (2007) The IL-4/IL-13/Stat6 signalling pathway promotes luminal mammary epithelial cell development. *Development* 134(15):2739–2750.
7. Alcaraz J, et al. (2008) Laminin and biomimetic extracellular elasticity enhance functional differentiation in mammary epithelia. *EMBO J* 27(21):2829–2838.
8. Paszek MJ, et al. (2005) Tensional homeostasis and the malignant phenotype. *Cancer Cell* 8(3):241–254.
9. Barocas VH, Moon AG, Tranquillo RT (1995) The fibroblast-populated collagen microsphere assay of cell traction force—Part 2: Measurement of the cell traction parameter. *J Biomech Eng* 117(2):161–170.

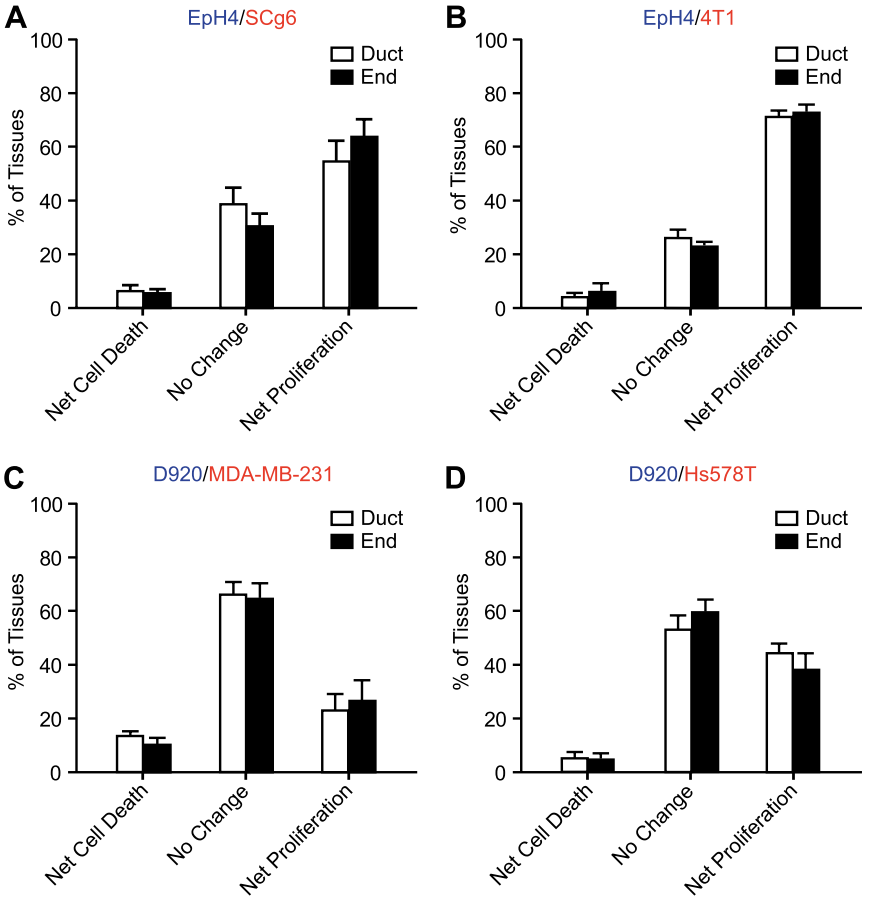

Fig. S1. Turnover of invasive tumor cells is not affected by initial location. Quantification of change in cell number based on initial position for (*A*) EpH4 and SCg6 cells, (*B*) EpH4 and 4T1 cells, (*C*) D920 and MDA-MB-231 cells, and (*D*) D920 and Hs578T cells. Error bar represents SEM ($n = 3$).

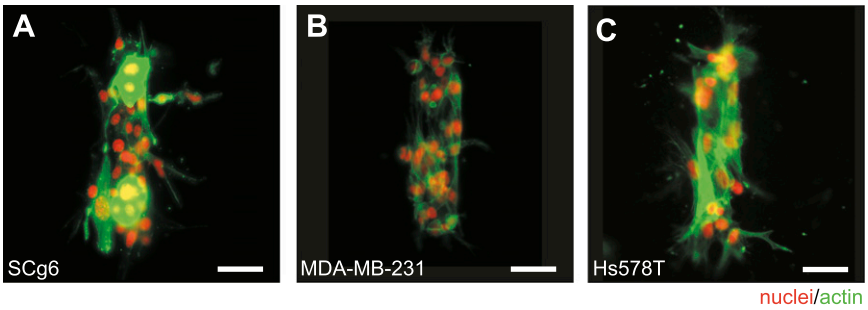

Fig. S2. Random invasion of tumor cell lines. (*A*) SCg6, (*B*) MDA-MB-231, and (*C*) Hs578T invade randomly in the absence of host epithelium. (Scale bar, 50 μm.)

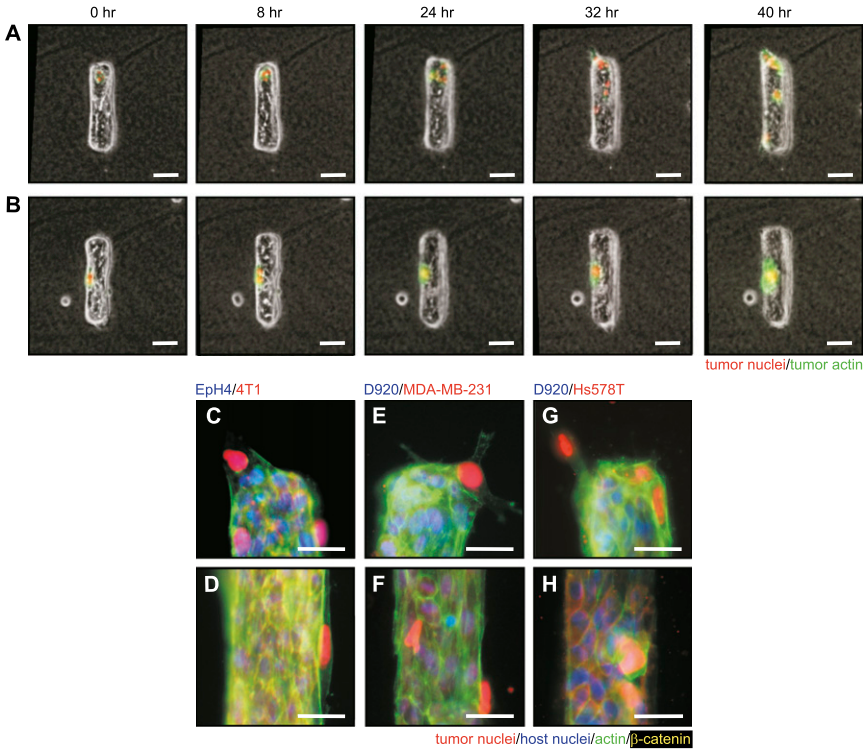

Fig. S3. Normal host architecture suppresses tumor cell invasion from the duct. Time-lapse images of an SCg6 invasive tumor cell (*A*) invading from the end, but (*B*) not invading from the duct of an EpH4 tissue. (Scale bars, 50 μm.) Fluorescence image of 4T1 cell (*C*) invading from the end but (*D*) not from the duct of an EpH4 tissue. MDA-MB-231 cell (*E*) invading from the end but (*F*) not from the duct of a D920 tissue. Hs578T cell (*G*) invading from the end but (*H*) not from the duct of a D920 tissue. (Scale bars, 25 μm.)

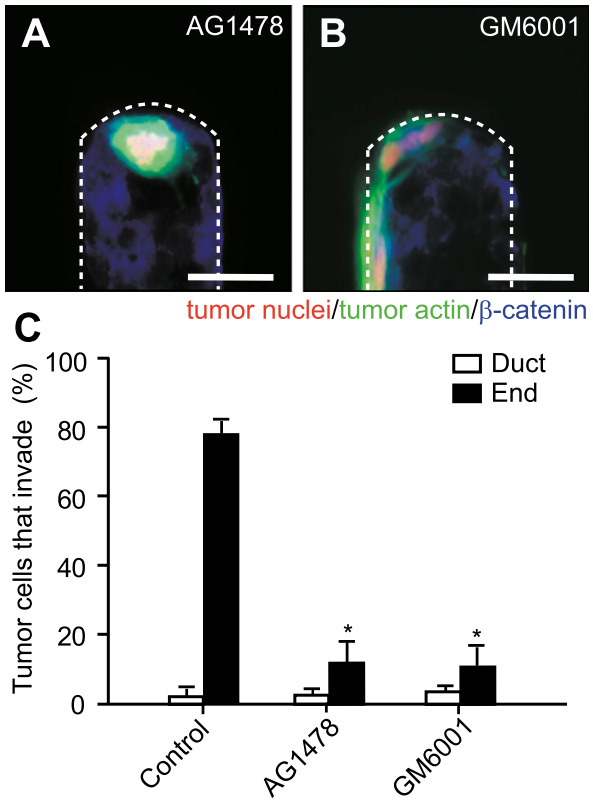

Fig. S4. Tumor cells require epidermal growth factor receptor (EGFR) and matrix metalloproteinases (MMPs) for invasion. SCg6 cells are inhibited from invading when tissues are treated with (*A*) AG1478, a pharmacological inhibitor of EGFR or (*B*) GM6001, a pharmacological inhibitor of MMP activity. (*C*) Quantification of invasion. Error bar represents SEM ($n = 3$). *P* values were calculated using a paired two-sided *t* test comparing each treatment to the control. $^*P < 0.05$.

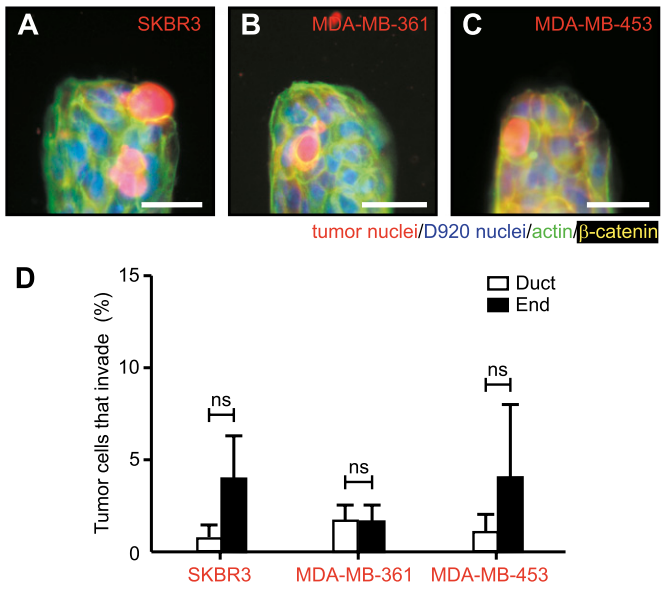

Fig. S5. Noninvasive tumor cells are not induced to invade. Shown for (*A*) SKBR3, (*B*) MDA-MB-361, and (*C*) MDA-MB-453 tumor cells lines in a D920 host tissue. (Scale bars, 25 μm.) (*D*) Quantification of invasion. Error bar represents SEM ($n = 3$).

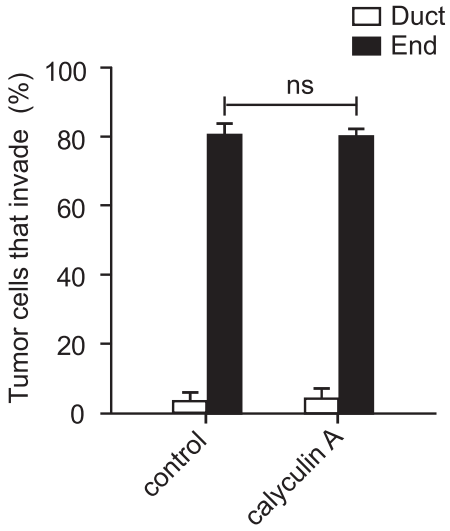

Fig. S6. Increasing contractility with calyculin A does not increase invasion. Error bars represent SEM (n = 3).

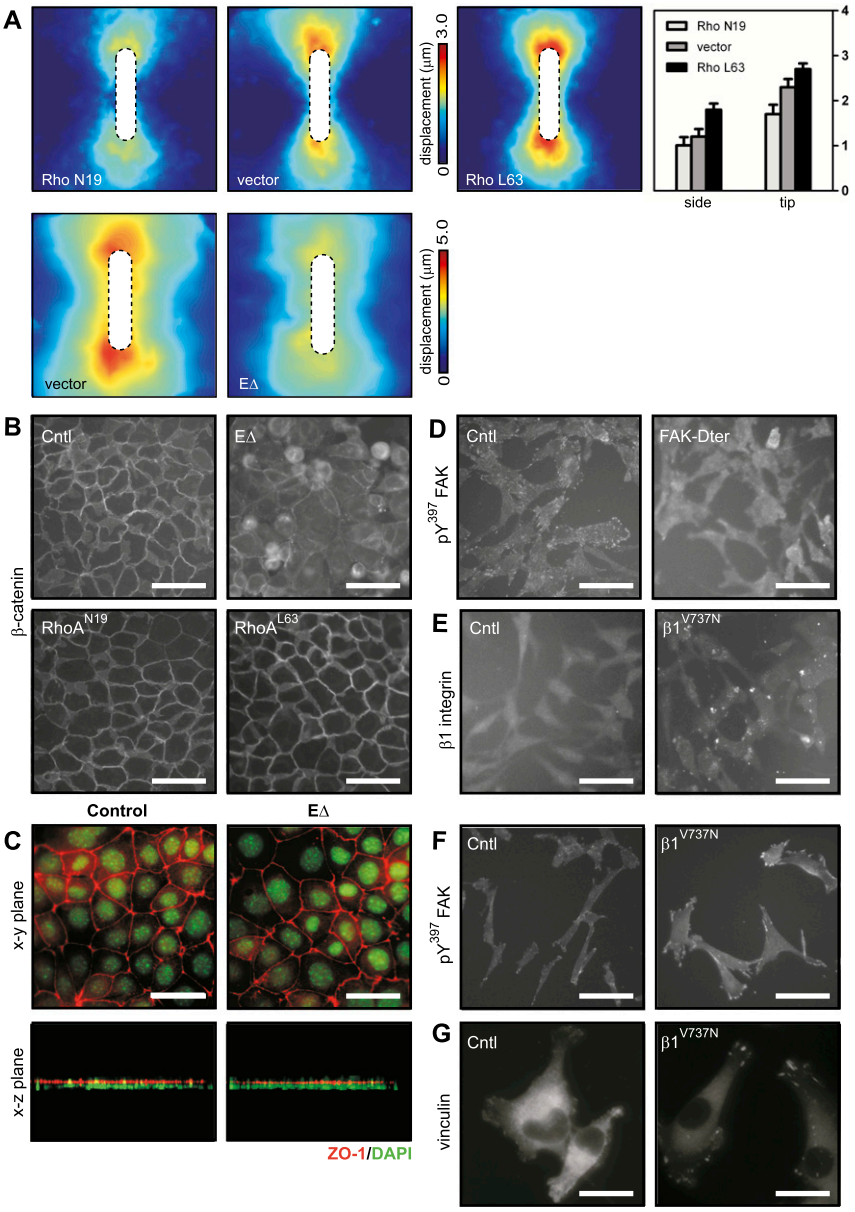

Fig. S7. Virus transduction and plasmid transfection. (*A*) Expression of $RhoA^{L63}$ increases tissue contractility; conversely, expression of EΔ or $RhoA^{N19}$ decreases tissue contractility, as inferred from bead displacements. (*B*) Expression of β-catenin in control EpH4 mammary epithelial cells and cells expressing EΔ, $RhoA^{N19}$, and $RhoA^{L63}$. (*C*) Expression of EΔ does not alter cell polarity. ZO-1 is localized primarily at the apical side of both control cells and cells expressing EΔ. (*D*) Expression of pY^{397} FAK in control SCg6 tumor cells and cells expressing FAK-Dter. Expression of (*E*) β1-integrin, (*F*) pY^{397} FAK, and (*G*) vinculin in SCg6 (*E* and *F*) or MDA-MB-231 (*G*) tumor cells and cells expressing $β1^{V737N}$. (Scale bars, 50 μm in *B*–*F* and 20 μm in *G*.)

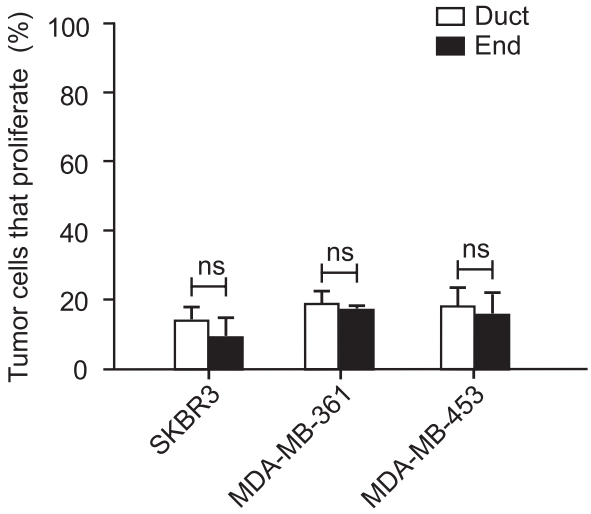

Fig. S8. Blocking intercellular transmission of mechanical stress inhibits preferential proliferation of noninvasive tumor cells. Quantification of EdU incorporation by SKBR3, MDA-MB-453, and MDA-MB-361 cells in host tissues comprised of D920 cells expressing EΔ. Error bars represent SEM (n = 3).

Table S1. Overview of tumor cell lines used

Cell line	3D morphology	ER/PR/HER2	Tumor type	p53	Ras	Invasive
SCg6	S	*/*/+	N/A	*	*	+
4T1	G/S	*/*/–	N/A	*	*	+
Hs578T	S	–/–/–	IDC	M	M	+
MDA-MB-231	S	–/–/–	AC	M	M	+
MDA-MB-361	G	+/+/+	AC	WT	WT	–
MDA-MB-453	G	–/–/+	AC	WT	WT	–
SKBR3	G	–/–/+	AC	M (1)	WT (2)	–

Adapted from refs. 3 and 4. 3D morphology: S, stellate; G, grape-like. ER/PR/HER2: + represents ER and PR expression or HER2 amplification. Tumor type: IDC, invasive ductal carcinoma; AC, adenocarcinoma. M, mutant. *Information not available.

1. Blagosklonny MV, et al. (2001) Inhibition of HIF-1- and wild-type p53-stimulated transcription by codon Arg175 p53 mutants with selective loss of functions. *Carcinogenesis* 22(6): 861–867.
2. Joseph EW, et al. (2010) The RAF inhibitor PLX4032 inhibits ERK signaling and tumor cell proliferation in a V600E BRAF-selective manner. *Proc Natl Acad Sci USA* 107(33):14903–14908.
3. Neve RM, et al. (2006) A collection of breast cancer cell lines for the study of functionally distinct cancer subtypes. *Cancer Cell* 10(6):515–527.
4. Kenny PA, et al. (2007) The morphologies of breast cancer cell lines in three-dimensional assays correlate with their profiles of gene expression. *Mol Oncol* 1(1):84–96.